

Article

Influence of the Addition of Rare Earth Elements on the Energy Storage and Optical Properties of $\text{Bi}_{0.5}\text{Na}_{0.5}\text{TiO}_3\text{-}0.06\text{BaTiO}_3$ Polycrystalline Thin Films

Ilham Hamdi Alaoui , Mebarki Moussa, Nathalie Lemée, Françoise Le Marrec, Anna Cantaluppi, Delphine Favry and Abdelilah Lahmar * 

Laboratory of Condensed Matter Physics, University of Picardie Jules Verne, 33 Rue Saint Leu, 80039 Amiens, France

* Correspondence: abdel.ilah.lahmar@u-picardie.fr; Tel.: +33-3-22-82-76-91

Abstract: Rare earth element-doped $\text{Bi}_{0.5}\text{Na}_{0.5}\text{TiO}_3\text{-BaTiO}_3$ (BNT–BT–RE) polycrystalline thin films were processed on a platinized substrate by chemical solution deposition. The microstructure, dielectric, and ferroelectric properties were investigated for all prepared films. It was found that the incorporation of rare earth elements into the BNT–BT matrix increases both the dielectric constant and the breakdown strength while maintaining low dielectric losses, leading to an enhancement of the energy storage density to $W_{rec} = 12$ and 16 J/cm^3 under an effective field of $E = 2500 \text{ kV/cm}$, for Nd- and Dy-based films, respectively. The optical properties of films containing the lanthanide element were investigated and the obtained results bear interest for luminescence applications. The simultaneous appearance of ferroelectric and optical properties in the system under investigation is very promising for advanced optoelectronic devices.

Keywords: BNT–BT thin films; rare earth addition; photoluminescence; dielectric measurements; energy storage



Citation: Alaoui, I.H.; Moussa, M.; Lemée, N.; Le Marrec, F.; Cantaluppi, A.; Favry, D.; Lahmar, A. Influence of the Addition of Rare Earth Elements on the Energy Storage and Optical Properties of $\text{Bi}_{0.5}\text{Na}_{0.5}\text{TiO}_3\text{-}0.06\text{BaTiO}_3$ Polycrystalline Thin Films. *Materials* **2023**, *16*, 2197. <https://doi.org/10.3390/ma16062197>

Academic Editors: Yuhang Ren and Jun Ouyang

Received: 6 February 2023

Revised: 28 February 2023

Accepted: 6 March 2023

Published: 9 March 2023



Copyright: © 2023 by the authors. Licensee MDPI, Basel, Switzerland. This article is an open access article distributed under the terms and conditions of the Creative Commons Attribution (CC BY) license (<https://creativecommons.org/licenses/by/4.0/>).

1. Introduction

Energy storage may take various forms, electrochemical, thermal, mechanical, etc. However, in electrical and electronic systems, energy storage requirements come into play in two fundamental ways: the first concerns the use of longer-term electrostatic discharges including energy supply in the case of redundant energy sources. The second is short-term storage, where components of electrically powered circuits store energy in an electrostatic or electromagnetic form [1]. Capacitors and inductors are typical examples. Recently, a revival of interest is devoted to lead-free dielectric capacitors for electrostatic energy storage [2–11]. Attracted by their ultra-fast charging–discharging characteristics combined with their high-power density, the industrial and research communities focus their efforts on chapping environmentally friendly materials able to meet the needs of modern technology [12]. Antiferroelectric materials are best suited for energy storage because they have high saturation polarization, low residual polarization, and low dielectric losses [13,14]. Unfortunately, most of these materials are lead-based, which is toxic and harmful to human health and the environment [15]. Alternatively, ferroelectric relaxors can also store a large amount of electrical energy because they have a slim hysteresis loop and a large saturation polarization, and a high coercive field [16–21].

Among the interesting lead-free perovskites, $\text{Bi}_{0.5}\text{Na}_{0.5}\text{TiO}_3$ (abbreviated as BNT) has been paid a great deal of attention, owing to its excellent ferroelectric properties and also the presence of a likely antiferroelectric phase transition called the depolarization transition (T_d). BNT was reported to exhibit an A-site disorder with the simultaneous presence of both Na and Bi elements [22]. It has been demonstrated in several works using advanced

characterization tools such as X-ray and electron diffraction techniques, that at room temperature, BNT is considered to be of cubic symmetry with rhombohedral $R3c$ and tetragonal $P4bm$ polar nanoregions, albeit a dominating of $R3c$ can be spotted at RT. However, in the temperature-dependent dielectric permittivity, a shoulder is observed around T_d , which is promoted only in the case of substitution or polling, resulting from a mixed contribution from $R3c$ -to- $P4bm$ polar nanoregions transition [23]. Around this transition, BNT-based materials exhibit double-pinched ferroelectric hysteresis loops [2,4,5,23]. The origin of this behavior has been widely discussed in the literature [24,25].

Unfortunately, the pure BNT phase exhibits a large coercive field ($E_C = 73$ kV/cm) as well as high dielectric losses leading to a small breakdown field, which limits its consideration for energy storage [1,5]. Thus, the compositional modulation by substitution in the pure BNT was found to be a good strategy for overcoming these drawbacks.

For instance, several BNT-based ceramic materials are reported to endorse interesting energy density (W_{rec}). The focus was on how to increase the dielectric breakdown to increase the stored energy, although, the obtained energy remains below expectations for the technological applications. This is why particular interest has been directed toward thin films of these materials in which a high dielectric breakdown field can be reached [4]. The review of the literature shows that the energy stored in thin films greatly exceeds that of ceramics by many orders of magnitude [26–28]. Adjusting the composition close to the morphotropic boundary phase (MBP) of BNT-BaTiO₃ (BNT–BT) was found to be an appropriate way to improve the stored energy. Yuan Yao et al. [9] reported a $W_{rec} = 32$ J/cm³ for 0.9(0.94Bi_{0.5}Na_{0.5}TiO₃-0.06BaTiO₃)-0.1NaNbO₃ thin films deposited on LaNiO₃ using a radio-frequency (RF) magnetron sputtering technique. Further, an ultrahigh recoverable energy storage density of about 54 J/cm³ was reported for Mn-modified BNT–BT thin films prepared by chemical solution deposition [7]. In this perspective, we have investigated the addition of rare earth elements to this MBP composition to increase the stored energy and to also take advantage of the presence of lanthanide elements to highlight luminescence properties. The simultaneous occurrence of ferroelectric and optical properties in the studied system holds great promise for optoelectronic and photonic applications.

2. Materials and Methods

Bismuth acetate (III) (C₆H₉BiO₆), Sodium acetate (C₂H₃NaO₂), Barium acetate (Ba(C₂H₃O₂)₂), rare earth acetate RE(O₂C₂H₃)₃ (RE = Nd; Dy), and titanium isopropoxide (C₁₂H₂₈O₄Ti) were used as starting materials to prepare a 0.3 mol/L precursor solution. Firstly, Bi, Ba, Na, and RE acetates were dissolved in acetic acid with appropriate stoichiometry. Separately, Ti-isopropoxide was dissolved in 2-Methoxyethanol and stabilized with acetylacetone (AcAc) selected as a chelating agent. Finally, the two solutions were mixed and stirred to yield a stable solution at room temperature. Thin film fabrication was performed by multiple-layer deposition using spin-coating onto Pt/SiN substrates. The pyrolysis of each layer was carried out on a hotplate at 400 °C for 10 min. The crystallization of the prepared films was carried out in a tube furnace at 600 °C under an O₂ atmosphere for 30 min. The final thickness was estimated to be around 460 nm.

An FEI Quanta 200 FEG Environmental SEM was used to analyze the microstructure of the investigated thin films. The phase purity was checked by X-ray diffraction using a four-circle Bruker Discover Advance D8 diffractometer with CuK $\alpha = 1.5406$ Å. Raman spectroscopy was performed using a Renishaw micro-Raman spectrometer under a green laser excitation wavelength of 514.5 nm. The dielectric investigations were conducted using a Solartron Impedance analyzer SI-12060. A ferroelectric test system (TF Analyzer 2000, aixACCT, Aachen, Germany) was used to collect P–E hysteresis loops. Finally, the luminescence properties were investigated using a LabRAM HR Evolution spectrophotometer under an excitation laser wavelength of 360 nm for the Dy phase and 786 nm for the Nd phase.

3. Results

3.1. Microstructural and Structural Investigations

Figure 1 shows scanning electron microscopy images for the investigated samples. The films were crack-free, dense, and fine-grained. As can be seen from Figure 1b,c, doping with rare earth elements induced a reduction in the grain size compared to the BNT–BT films. The average grain size in undoped BNT–BT was found to be $0.62\ \mu\text{m}$, which is much larger than that observed in doped films— $0.38\ \mu\text{m}$ and $0.36\ \mu\text{m}$ for BNT–BT–Dy and BNT–BT–Nd, respectively. A similar behavior was reported by Yanjiang Xie et al. [7] while adding Mn to the BNT–BT polycrystalline thin films. They attributed this behavior to the “solute drag” effect. The authors surmised that the nonuniform distribution of the doping element into the host matrix leads to the reduction in the driving force for grain boundary migration. The inhibition of grain growth by the incorporation of rare earth elements has been reported in many types of research work [4]. A typical cross-section of one of these films is presented in Figure 1d, revealing a uniform thickness of about $463\ \text{nm}$. For doped films, the thickness was found to be around $472\ \text{nm}$ and $475\ \text{nm}$ for Dy and Nd-based films, respectively.

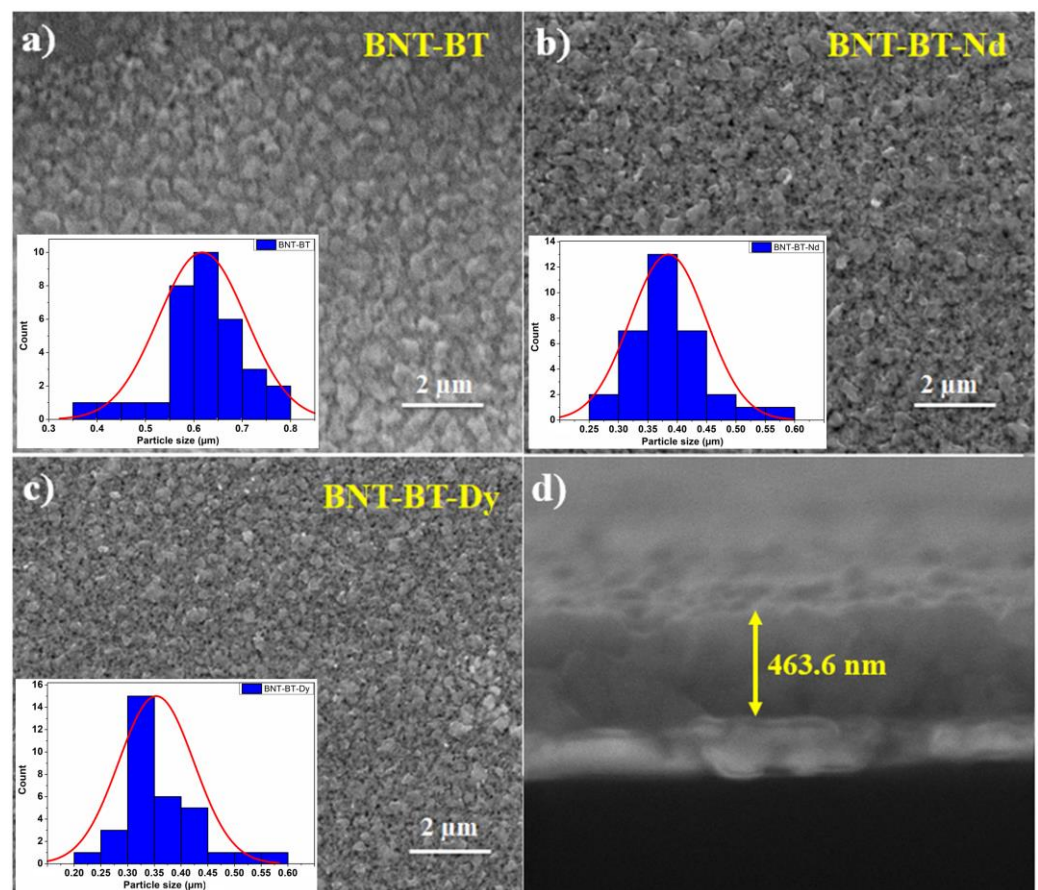


Figure 1. SEM images showing the microstructure of the investigated thin films: (a) BNT–BT, (b) BNT–BT–Nd, (c) BNT–BT–Dy, and (d) example of a cross-sectional image of the BNT–BT thin film.

Figure 2 presents the EDX spectra for the compositional distribution in the investigated films. As expected, the characteristics of starting elements Bi, Na, Ba, Ti, and O, are detected for all samples. Further, the supplementary lanthanide element is detected in the doped films, which confirms the successful inclusion of Nd and Dy elements into the BNT–BT matrix.

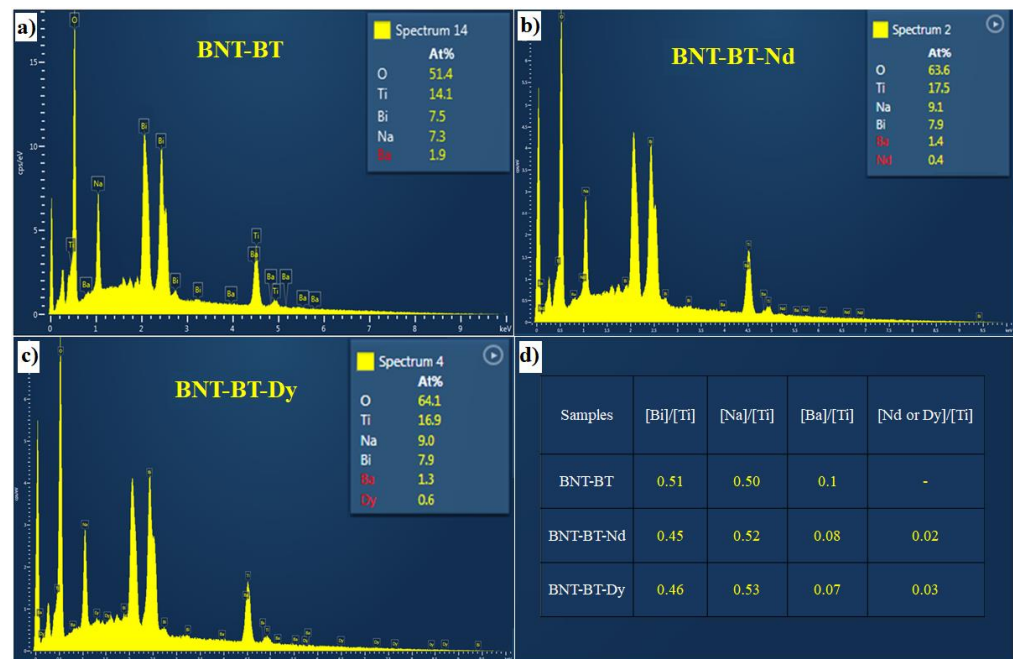
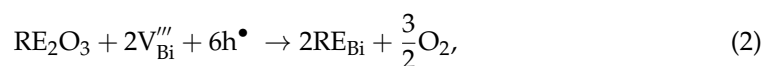


Figure 2. EDX spectra with the atomic percentage of (a) BNT-BT, (b) BNT-BT-Nd, (c) BNT-BT-Dy, and (d) table of atomic ratios.

Figure 3 shows the XRD diagrams of BNT-BT and lanthanide-doped BNT-BT films. The zoom on the reflection around the first order of the substrate clearly shows the existence of a splitting of the film's peak on both sides of 40° (Figure 3a). These two peaks seem to be related to the film and not to the substrate. To obtain further information about this splitting, the grazing incidence mode (GI) was used to eliminate the substrate contribution, as shown in Figure 3b. The obtained XRD patterns were indexed based on the rhombohedral BNT and the tetragonal BT. The coexistence of rhombohedral $R3c$ and tetragonal $P4bm$ has already been highlighted in several works to be around $x = 0.6$ (MBP region) [29,30]. The splitting of the $(202)_{\text{BNT}}$ peak (indexed in rhombohedral NBT) to two peaks $(002)_{\text{BT}}$ and $(200)_{\text{BT}}$ (indexed in tetragonal BaTiO_3) and the combination of $(003)_{\text{BNT}}$ and $(021)_{\text{BNT}}$ into only one peak was reported as a signature of the complete transformation from the $R3c$ phase to the $P4mb$ phase. In this study, the splitting was achieved; but not the combination, which confirms the coexistence of both rhombohedral and tetragonal phases.

3.2. Dielectric Investigations

The frequency dependence of the dielectric constant and dielectric loss of BNT-BT and BNT-BT-RE (Dy and Nd) thin films at room temperature are plotted in Figure 4. The beneficial effect of the addition of lanthanide on the dielectric properties can be seen clearly. The dielectric constant increased from 600 for the BNT-BT phase to around 1000 for films containing rare earth elements; this behavior may be linked to the reduction in oxygen vacancies formed by the Bi volatility. In this case, the substitution of Bi by a nonvolatile lanthanide element should reduce the number of vacancies, according to the following equations (using Vink–Kröger notation):



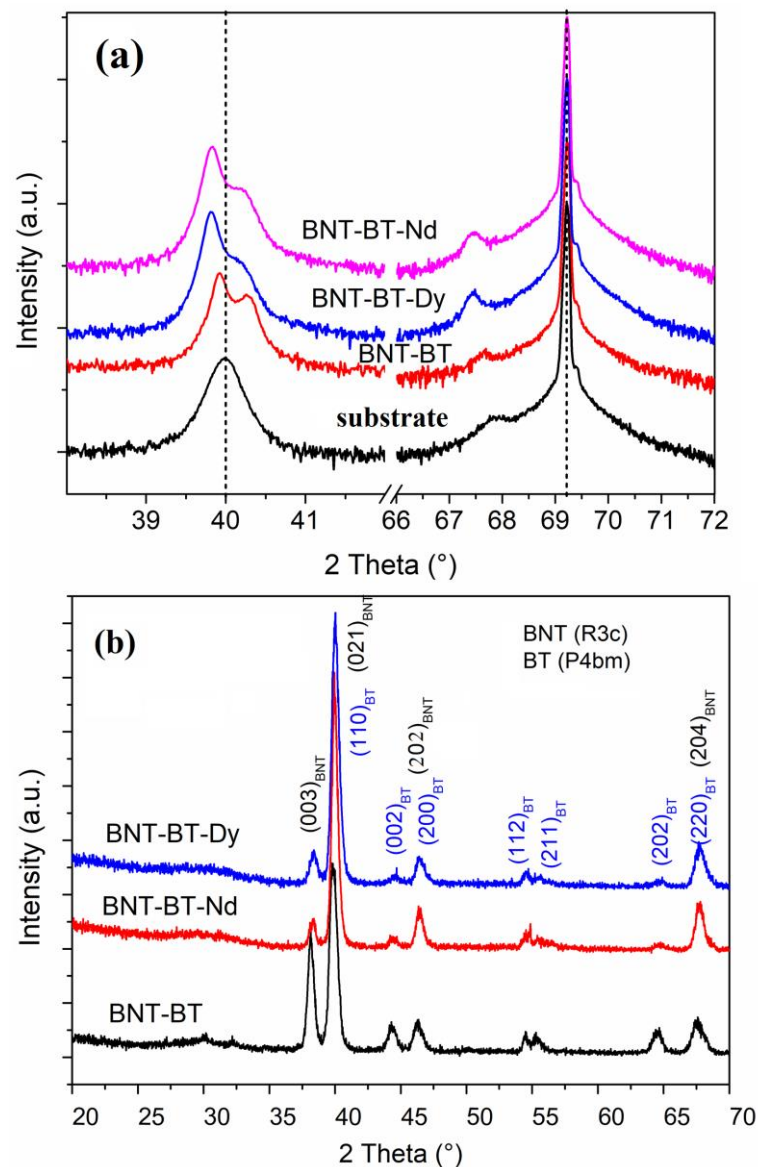


Figure 3. (a). Room-temperature X-ray diffractograms of BNT-BT, BNT-BT-RE (RE = Nd and Dy), and of the substrate, with a zoom of the X-ray diffraction patterns around 40° and 69° , and (b) X-ray diffractograms of the investigated films measured under grazing incidence mode.

Figure 5 displays the thermal variation in the dielectric constant and dielectric loss for the investigated samples. No clear dielectric anomalies were depicted from the plot of BNT-BT and BNT-BT-Dy; only humps were observed. To highlight the possible phase transitions around these humps, the differential curves of the dielectric constant ($\partial\epsilon_r/\partial T$) as a function of temperature were plotted in the inset of Figure 5a. As can be seen from the plots, a visible anomaly is observed at around 120°C that could be attributed to the depolarization temperature (T_d). In contrast, the BNT-BT-Nd film shows one visible dielectric transition at $T_m = 270^\circ\text{C}$.

A maximum around this temperature is observed for BNT-BT thin films with Na and/or Bi excess around the MBP composition [31]. It is worth mentioning that in bulk BNT-xBT solid solutions near the MBP, Badapanda et al. reported that the two observed anomalies (T_d and T_m) merged into one for the composition $x = 0.8$, then appeared again for $x = 0.9$. The authors have considered $x = 0.8$ as the highest MBP composition [32]. Figure 5b exhibits the frequency dependence of the thermal variation in the dielectric loss for BNT-BT. A clear relaxation phenomenon is observed that agrees well with the reported

bibliography [23,24,26,29,31]. Note that similar behavior is observed for doped films (not shown here).

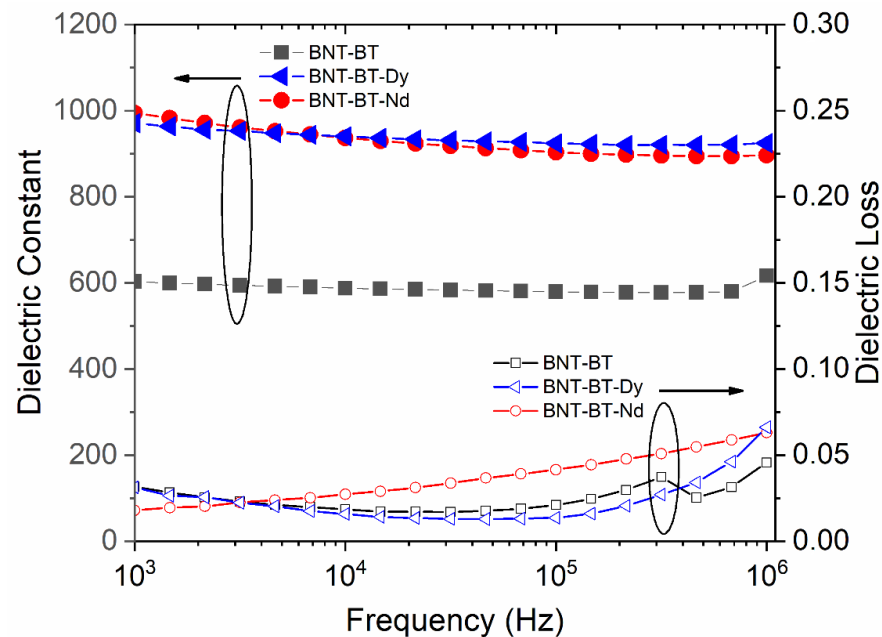


Figure 4. Room-temperature frequency dependence of the dielectric constants and the dielectric losses for the investigated samples.

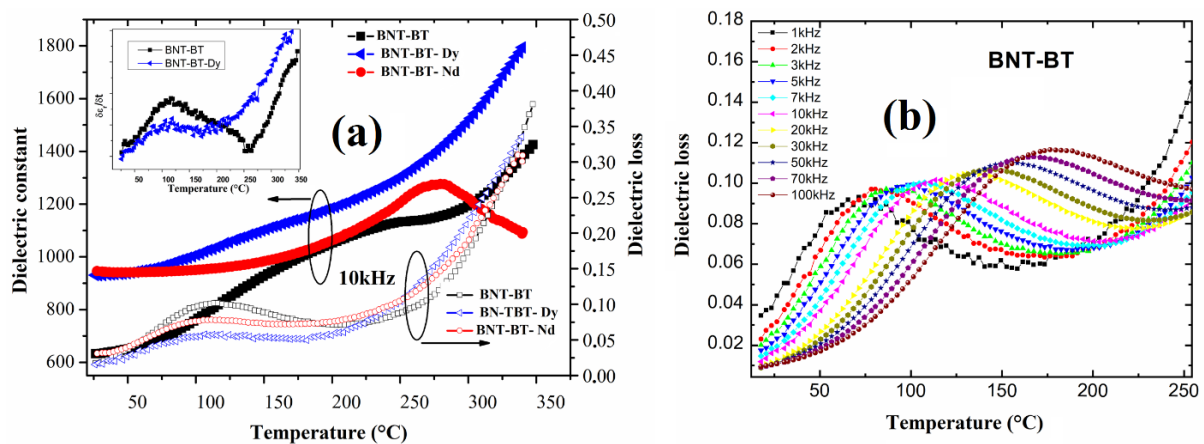


Figure 5. (a). Variation in the dielectric constant and the dielectric loss as a function of temperature for the investigated samples. The inset shows the derivative of the dielectric constant versus temperature for BNT-BT and BNT-BT-Dy compositions, and (b) an example of frequency dependence of the thermal variation in the dielectric loss for BNT-BT thin films.

3.3. Ferroelectric and Energy Storage Investigations

Figure 6a shows the P - E hysteresis loop of the parent BNT-BT matrix of composition $x = 0.06$ located in the MBP region. The obtained P - E loop is characterized by a linear and slim shape. It is noted that the increase in the applied field does not induce polarization saturation; only an increase in the linearity of the hysteresis loop is observed. In a previous work [2,4], we found that the inclusion of lanthanide elements in the BNT matrix led to changes in the order of the A/B-site cations, which induced local random fields and thus a structural heterogeneity, useful for improving the energy storage properties.

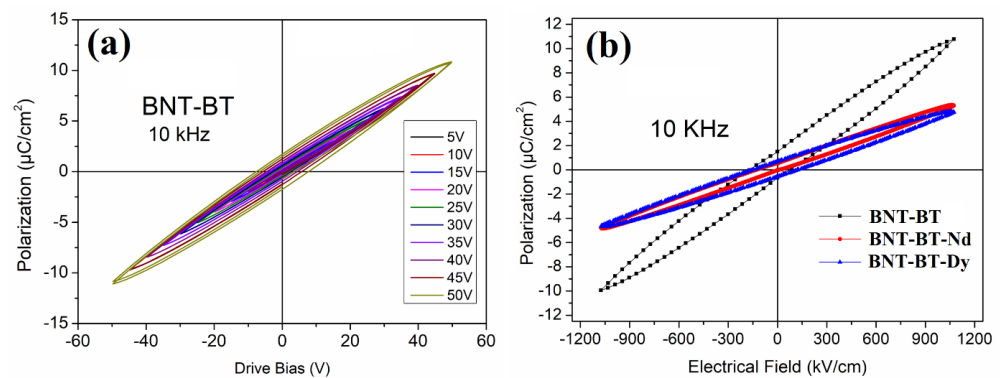


Figure 6. *P-E* hysteresis loops at room temperature for (a) BNT-BT thin films under different applied biases, and (b) the comparison of undoped and doped thin films at a 10 kHz test frequency.

Indeed, depending on the amount of RE doping into BNT (a non-ergodic relaxor material), different relaxation states could be obtained until a paraelectric-like state is achieved.

In this work, we surmise the coexistence of the ergodic and non-ergodic in BNT-BT caused by the $R3c$ and $P4mb$ nanopolar competition, which causes local random fields that break the long-range ferroelectric order instead of a short-range polar order. This is in good agreement with the X-ray diffraction investigation, where this competition is highlighted by the presence of rhombohedral and tetragonal diffraction peaks. Figure 6b shows the comparison of the *P-E* loops of undoped and doped BNT-BT thin films. The obtained slim hysteresis loop is a signature of the complete ergodic relaxor phase [4,5]. In fact, the substitution of Bi by Ba in the BNT matrix promotes the room-temperature relaxor properties, which is in good agreement with the result obtained in the dielectric investigations (Figure 5b). In addition, the introduction of the additional Bi substitution (inclusion of the RE elements) results in an increased disorder within the structure and, consequently, the relaxor behavior is amplified, leading to a decrease in the remanent polarization, and the hysteresis becomes slimmer.

The energy storage properties of the prepared thin films can be determined using the *P-E* loops by the integration of the polarization versus the electric field using the following equation:

$$W_{rec} = \int_{P_r}^{P_m} E dP, \quad (3)$$

The condition to obtain a high energy storage density is to have a high $\Delta P = P_m - P_r$ value as well as a high breakdown electric field value. Energy efficiency is an interesting parameter to evaluate the discharge property. It can be determined using the following equation:

$$\eta = \frac{W_{rec}}{W_{rec} + W_{loss}} \times 100, \quad (4)$$

where

$$W_{loss} = W_{stored} - W_{rec}, \quad (5)$$

It is noted that the condition of high energy efficiency simultaneously requires a high recovered energy and a low lost energy (Figure 7a).

The energy storage parameters were determined versus different values of the applied field in the positive part of the hysteresis loops (Figure 7b–d). Table 1 summarized the calculated parameter for the studied thin films in a comparison with reported data in the literature.

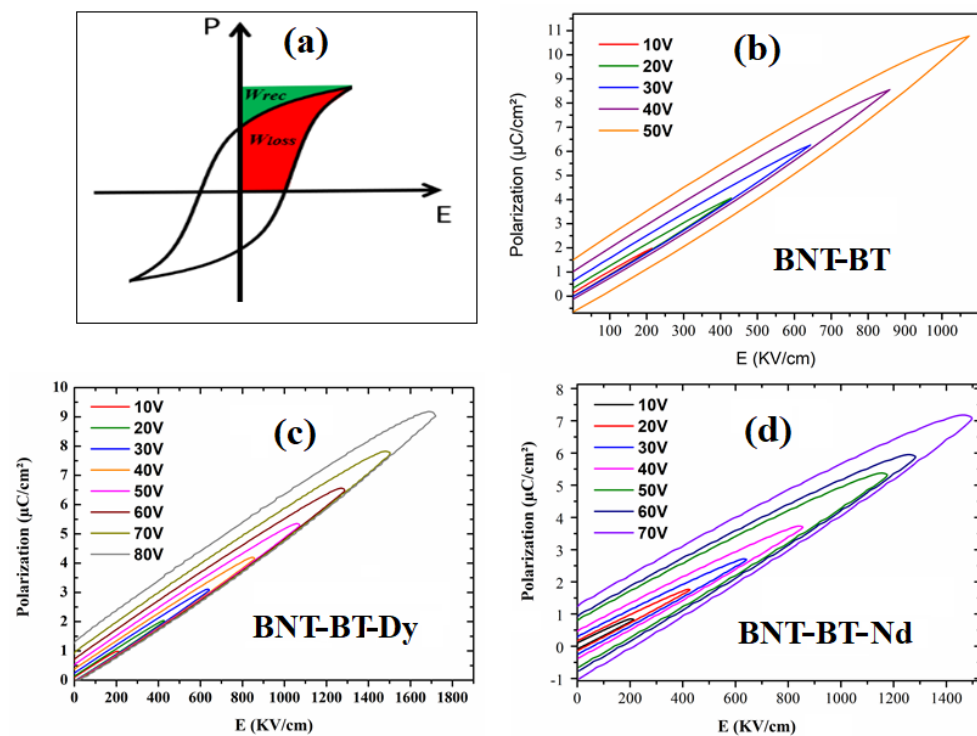


Figure 7. (a) Definition of the energy storage parameters; P-E hysteresis loops at room temperature in the positive part of the P-E loops: (b) BNT-BT, (c) BNT-BT-Dy, and (d) BNT-BT-Nd thin films.

Table 1. Comparison of the energy storage parameters of the investigated thin films with some reported bibliographic data on BNT-based thin films.

Samples	E_{\max} (kV/cm)	W_{rec} (J/cm ³)	η (%)	Ref.
BNT-BT	1080 (real)	4.5	45	This work
BNT-BT-xNd (x = 0.01)	1080 (real)	2	68	This work
	1780 (real)	5.3	59	
	2500 (effective)	12	58	
BNT-BT-xDy (x = 0.01)	1080 (real)	2.5	79	This work
	1780 (real)	6.6	72	
	2500 (effective)	16	64	
BNT-BT-xMn (x = 0.2)	2000	25	82	[7]
BNT-BT-xMn (x = 0.6)	2500	54	59	[7]
BNT-xHo (=0.02)	500	9.4	55	[2]
BNT-xEr (=0.02)	500	9.2	57	[2]
BNT-BT-NaNbO ₃ (=0.1)	3170	32	90	[9]
6BNT-4ST	10.4	64.5	64.5	[10]
0.94BNT-0.06BT with PLCT seed layers	17.2	74.3	74.3	[30]

Figure 8 shows the variation in W_{rec} and η as a function of the applied electric field for all investigated films. It can be seen from the plots that W_{rec} increases with an increasing applied electric field. However, for BNT-BT films, it was not possible to apply a high electric field because of the breakdown effect. Contrarily, films containing elemental lanthanide exhibit high dielectric rigidity with a high breakdown electric field, which helps to increase the recovered energy density from 4.5 J/cm³ to around 6.5 J/cm³ for BNT-BT-Dy under $E = 1750$ kV/cm, noting that the breakdown field is not achieved because of the device limitation.

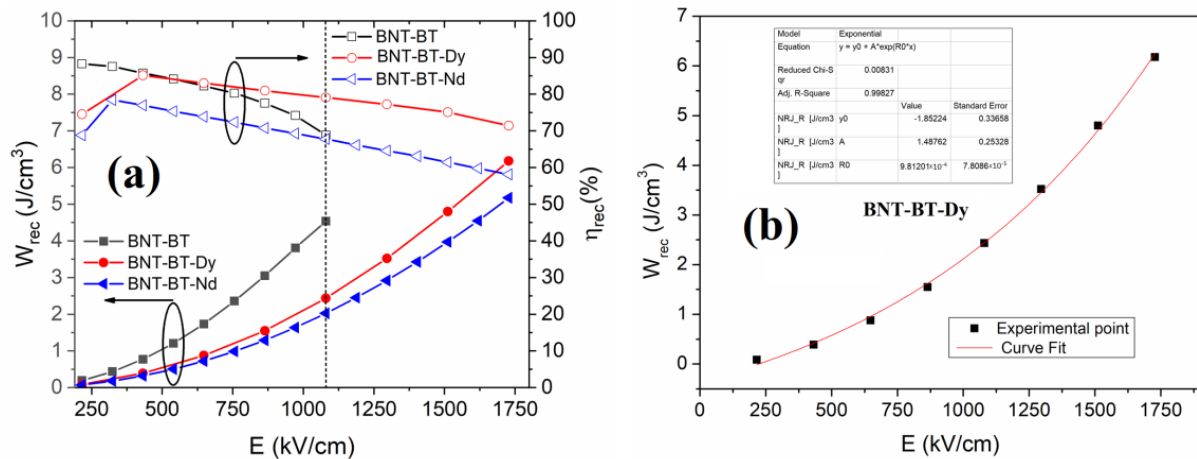


Figure 8. (a) Evolution of the energy storage parameters versus field density, and (b) Exponential fit of the experimental data for BNT-BT-Dy thin films.

We have attempted to numerically adjust the curves obtained for the two films doped with the rare earth element using an exponential function, as expressed by Equation (6), which perfectly fits both curves:

$$y = Ae^{R_0x} + y_0, \quad (6)$$

It is worth noting that in BNT-BT-Mn thin films, which are equivalent to the films investigated here, Yanjiang Xie et al. reported the possibility of applying a field of 2500 kV/cm reaching $W_{rec} = 54 \text{ J/cm}^3$. We have taken this value as the maximum effective field that can be applied to our system. Replacing this value in Equation (6) allowed us to determine energy values of $W_{rec} = 12$ and 16 J/cm^3 for Nd and Dy films, respectively. The efficiency in this field has also been determined by linear fitting and was found equal to 58% and 64%, respectively.

3.4. Optical Investigations

Figure 9 shows the room-temperature emission spectra for the BNT-BT doped with a lanthanide element after excitation with a suitable wavelength. The emission spectrum of BNT-BT-Dy is shown in Figure 9a. The measurement was performed with a UV excitation wavelength of $\lambda_{ext} = 360 \text{ nm}$. The obtained spectrum shows one intense emission at 573 nm, which corresponds to the $^4F_{9/2} \rightarrow ^6H_{13/2}$ transition. Two other weak emissions were observed at 475 and 649 nm, which are attributed to the transitions $^4F_{9/2} \rightarrow ^6H_{15/2}$ and $^4F_{9/2} \rightarrow ^6H_{11/2}$ [33].

The BNT-BT-Nd sample was excited with 786 nm and emitted in the near-infrared region (Figure 9b). Three clear bands were observed at 875, 1057, and 1505 nm. The diode emission observed at around 900 nm corresponds to the transition of $^4F_{3/2} \rightarrow ^4I_{9/2}$. It was attributed to the electronic transitions from the lowest $^4F_{3/2}$ crystal field component to the ground manifold [34]. We noted the observation of only two $^4I_{9/2}$ Stark levels instead of the expected five. The highest peak at 1057 nm was associated with the $^4F_{3/2} \rightarrow ^4I_{11/2}$ electronic transition. A very small emission was detected at 1324 nm, which was attributed to the $^4F_{3/2} \rightarrow ^4I_{13/2}$ transition. Finally, an intense band was observed at 1505 nm, which might be due to $^4F_{3/2} \rightarrow ^4I_{15/2}$; such a transition is not usually observed and could be promising for Mid-IR lasing [35].

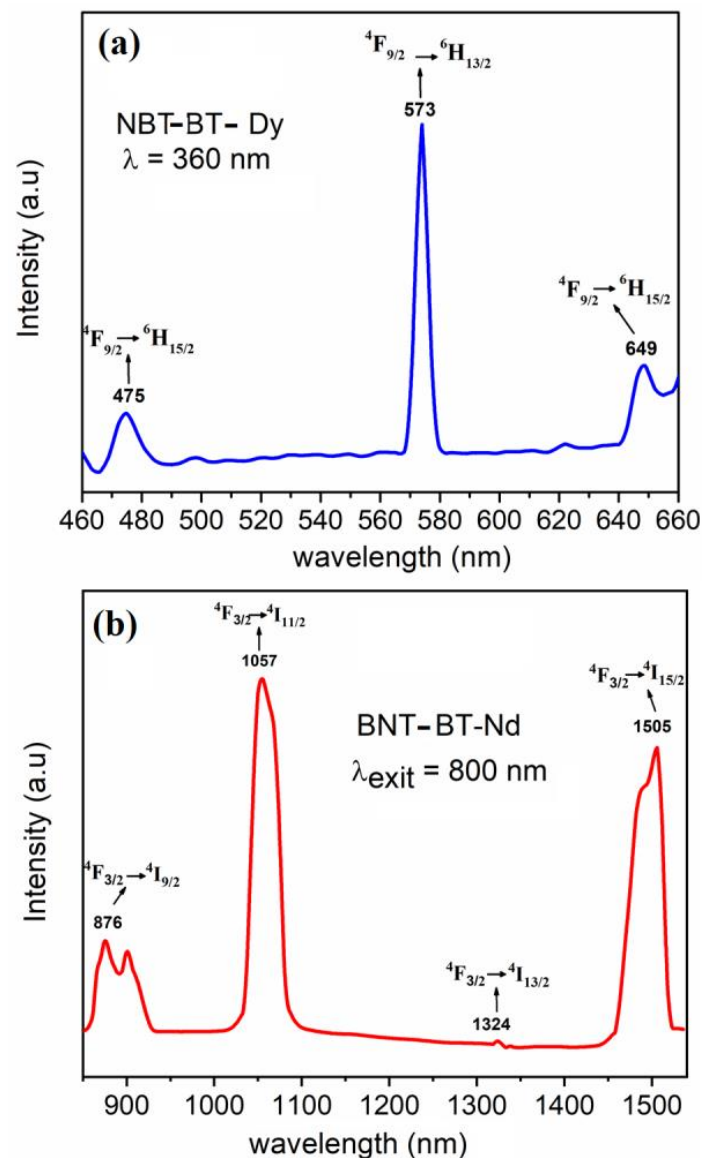


Figure 9. The emission spectrum of (a) BNT-BT-Dy after excitation at $\lambda_{\text{ext}} = 360$ nm, and (b) BNT-BT-Nd excited at $\lambda_{\text{ext}} = 800$ nm.

4. Conclusions

In summary, BNT-BT and BNT-BT-RE thin films were processed on a Pt/SiN substrate via chemical solution deposition. The incorporation of rare earth elements was found to improve the microstructure and decrease, by half, the average grain size, which considerably improved the electrical properties. X-ray diffractograms of the investigated films measured under grazing incidence mode confirmed the coexistence of both rhombohedral and tetragonal phases in all investigated films. The thermal variations in the dielectric constant revealed the presence of humps at around 120 °C for both BNT-BT and BNT-BT-Dy films, corresponding to the depolarization temperature. BNT-BT-Nd films exhibited one visible transition at 270 °C, which might be attributed to the complete $P4bm$ transition. Such behavior is compatible with the highest MBP composition. All films showed an unsaturated hysteresis loop, characteristic of the complete ergodic relaxor phase. Moreover, films containing rare earth elements were found slimmer and endorse high energy storage properties comparable with values reported so far in other BNT-based thin films.

For BNT-BT, the recoverable energy was found to be around 4.5 J/cm³ with an efficiency of 45%. The inclusion of rare earth elements was found to be beneficial for increasing the breakdown field, on the occurrence of the storage properties. Under an effective field of

2500 kV/cm, the calculated recoverable energy and efficiency were found to be 12 J/cm³ (58%) and 16 J/cm³ (64%) for BNT-BT-Nd and BNT-BT-Dy, respectively. They also presented some attractive photoluminescence properties. The simultaneous appearance of ferroelectric and optical properties in the system under investigation is very promising for advanced optoelectronic devices.

Author Contributions: Conceptualization, A.L. and N.L.; validation, A.L. and N.L.; formal analysis, I.H.A., M.M., A.C., and D.F.; investigation, A.C. and D.F.; data curation, I.H.A., M.M., and F.L.M.; writing—original draft preparation, A.L. and I.H.A.; writing—review and editing, N.L., F.L.M. and A.L.; supervision, A.L. and N.L. All authors have read and agreed to the published version of the manuscript.

Funding: This work was supported by the Region of Hauts de France Grant No. 20002828 (project OPPEN). I.H.A. acknowledges financial support from the Region of Hauts de France and the Amiens Metropole.

Institutional Review Board Statement: Not applicable.

Informed Consent Statement: Not applicable.

Data Availability Statement: Not applicable.

Conflicts of Interest: The authors declare no conflict of interest.

References

1. Nihal, K. *Energy Storage Devices for Electronic Systems: Rechargeable Batteries and Supercapacitors*; School of Engineering, The University of Waikato: Hamilton, New Zealand, 2015.
2. Zannen, M.; Belhadi, J.; Benyoussef, M.; Khemakhem, H.; Zaidat, K.; El Marssi, M.; Lahmar, A. Electrostatic energy storage in antiferroelectric like perovskite. *Superlattices Microstruct.* **2019**, *127*, 43–48. [[CrossRef](#)]
3. Benyoussef, M.; Belhadi, J.; Lahmar, A.; El Marssi, M. Tailoring the dielectric and energy storage properties in BaTiO₃/BaZrO₃ superlattices. *Mater. Lett.* **2019**, *234*, 279–282. [[CrossRef](#)]
4. Benyoussef, M.; Zannen, M.; Belhadi, J.; Manoun, B.; Kutnjak, Z.; Vengust, D.; Spreitzer, M.; El Marssi, M.; Lahmar, A. Structural, dielectric, and ferroelectric properties of Na_{0.5}(Bi_{1-x}Nd_x)_{0.5}TiO₃ ceramics for energy storage and electrocaloric applications. *Ceram. Int.* **2021**, *47*, 26539–26551. [[CrossRef](#)]
5. Benyoussef, M.; Zannen, M.; Belhadi, J.; Manoun, B.; Dellis, J.L.; El Marssi, M.; Lahmar, A. Dielectric, ferroelectric, and energy storage properties in dysprosium doped sodium bismuth titanate ceramics. *Ceram. Int.* **2018**, *44*, 19451–19460. [[CrossRef](#)]
6. Mezzourh, H.; Belkhadir, S.; Mezzane, D.; Amjoud, M.; Choukri, E.; Lahmar, A.; Gagou, Y.; Kutnjak, Z.; El Marssi, M. Enhancing the dielectric, electrocaloric and energy storage properties of lead-free Ba_{0.85}Ca_{0.15}Zr_{0.1}Ti_{0.9}O₃ ceramics prepared via sol-gel process. *Phys. B Condens. Matter* **2021**, *603*, 412760. [[CrossRef](#)]
7. Xie, Y.; Hao, H.; Xie, J.; Zhang, S.; Cao, M.; Yao, Z.; Liu, H. Ultra-high energy storage density and enhanced dielectric properties in BNT-BT based thin film. *Ceram. Int.* **2021**, *47*, 23259–23266. [[CrossRef](#)]
8. Chandrasekhar, M.; Khatua, D.K.; Pattanayak, R.; Kumar, P. Dielectric relaxation and conduction mechanism studies of BNT-BT-BKT ceramics. *J. Phys. Chem. Solids* **2017**, *111*, 160–166. [[CrossRef](#)]
9. Yao, Y.; Li, Y.; Sun, N.; Du, J.; Li, X.; Zhang, L.; Zhang, Q.; Hao, X. High energy-storage performance of BNT-BT-NN ferroelectric thin films prepared by RF magnetron sputtering. *J. Alloys Compd.* **2018**, *750*, 228–234. [[CrossRef](#)]
10. Kim, M.-K.; Ji, S.-Y.; Lim, J.-H.; Kim, S.-W.; Jeong, D.-Y. Energy storage performance and thermal stability of BNT-SBT with artificially modulated nano-grains via aerosol deposition method. *J. Asian Ceram. Soc.* **2022**, *10*, 196–202. [[CrossRef](#)]
11. Belarbi, M.; Tamraoui, Y.; Manoun, B.; Cantaluppi, A.; Gagou, Y.; Taibi, K.; El Marssi, M.; Lahmar, A. Structural, dielectric and energy storage properties of Neodymium niobate with tetragonal tungsten bronze structure. *Phys. B Condens. Matter* **2021**, *618*, 413185. [[CrossRef](#)]
12. Daniel, W.; Margieh, U. Energy Storage Capacitor Technology Comparison and Selection. In Proceedings of the 3rd PCNS, KYOCERA AVX, Milano, Italy, 7–10 September 2021; pp. 1–12. Available online: <https://epci.eu/energy-storage-capacitor-technology-comparison-and-selection/> (accessed on 6 February 2023).
13. Belhadi, J.; Hanani, Z.; Trstenjak, U.; Shepelin, N.A.; Bobnar, V.; Koster, G.; Hlinka, J.; Pergolesi, D.; Lippert, T.; El Marssi, M.; et al. Large imprint in epitaxial 0.67Pb(Mg_{1/3}Nb_{2/3})O₃-0.33PbTiO₃ thin films for piezoelectric energy harvesting applications. *Appl. Phys. Lett.* **2022**, *121*, 182903. [[CrossRef](#)]
14. Ait Tamerd, M.; Abraime, B.; El Rhazouani, O.; Lahmar, A.; El Marssi, M.; Hamedoun, M.; Benyoussef, A.; El Kenz, A. Modelling of the ferroelectric and energy storage properties of PbZr_{1-x}Ti_xO₃ thin films using Monte Carlo simulation. *Mater. Res. Express* **2019**, *6*, 126429. [[CrossRef](#)]
15. Radley-Gardner, O.; Beale, H.; Zimmermann, R. Directive 2011/83/EU of the European Parliament and of the Council. In *Fundamental Texts On European Private Law*; Hart Publishing: London, UK, 2020; pp. 629–665. [[CrossRef](#)]

16. Gao, F.; Dong, X.; Mao, C.; Liu, W.; Zhang, H.; Yang, L.; Cao, F.; Wang, G. Energy-Storage Properties of $0.89\text{Bi}_{0.5}\text{Na}_{0.5}\text{TiO}_3\text{-}0.06\text{BaTiO}_3\text{-}0.05\text{K}_{0.5}\text{Na}_{0.5}\text{NbO}_3$ Lead-Free Anti-ferroelectric Ceramics. *J. Am. Ceram. Soc.* **2011**, *94*, 4382–4386. [[CrossRef](#)]
17. Chandrasekhar, M.; Kumar, P. Synthesis and characterizations of BNT–BT and BNT–BT–KNN ceramics for actuator and energy storage applications. *Ceram. Int.* **2015**, *41*, 5574–5580. [[CrossRef](#)]
18. Yang, H.; Yan, F.; Lin, Y.; Wang, T.; Wang, F. High energy storage density over a broad temperature range in sodium bismuth titanate-based lead-free ceramics. *Sci. Rep.* **2017**, *7*, 8726. [[CrossRef](#)]
19. Wendari, T.P.; Arief, S.; Mufti, N.; Blake, G.R.; Baas, J.; Suendo, V.; Prasetyo, A.; Insani, A.; Zulhadjri, Z. Lead-Free Aurivillius Phase $\text{Bi}_2\text{LaNb}_{1.5}\text{Mn}_{0.5}\text{O}_9$: Structure, Ferroelectric, Magnetic, and Magnetodielectric Effects. *Inorg. Chem.* **2022**, *61*, 8644–8652. [[CrossRef](#)]
20. McCabe, E.E.; Bousquet, E.; Stockdale, C.P.J.; Deacon, C.A.; Tran, T.T.; Halasyamani, P.S.; Stennett, M.C.; Hyatt, N.C. Proper Ferroelectricity in the Dion–Jacobson Material $\text{CsBi}_2\text{Ti}_2\text{NbO}_{10}$: Experiment and Theory. *Chem. Mater.* **2015**, *27*, 8298–8309. [[CrossRef](#)]
21. Wang, H.; Gou, G.; Li, J. Ruddlesden–Popper perovskite sulfides $\text{A}_3\text{B}_2\text{S}_7$: A new family of ferroelectric photovoltaic materials for the visible spectrum. *Nano Energy* **2016**, *22*, 507–513. [[CrossRef](#)]
22. Davies, P.K.; Wu, H.; Borisevich, A.Y.; Molodetsky, I.E.; Farber, L. Crystal Chemistry of Complex Perovskites: New Cation-Ordered Dielectric Oxides. *Annu. Rev. Mater. Res.* **2008**, *38*, 369–401. [[CrossRef](#)]
23. Jo, W.; Schaab, S.; Sapper, E.; Schmitt, L.A.; Kleebe, H.J.; Bell, A.J.; Rödel, J. On the phase identity and its thermal evolution of lead free $(\text{Bi}_{1/2}\text{Na}_{1/2})\text{TiO}_3\text{-}6\text{ mol BaTiO}_3$. *J. Appl. Phys.* **2011**, *110*, 074106. [[CrossRef](#)]
24. Viola, G.; Ning, H.; Wei, X.; Deluca, M.; Adomkevicius, A.; Khaliq, J.; Reece, J.; Yan, H. Dielectric relaxation, lattice dynamics and polarization mechanisms in $\text{Bi}_{0.5}\text{Na}_{0.5}\text{TiO}_3$ -based lead-free ceramics. *J. Appl. Phys.* **2013**, *114*, 014107. [[CrossRef](#)]
25. Chu, B.J.; Chen, D.; Li, G.; Yin, Q. Electrical properties of $\text{Na}_{1/2}\text{Bi}_{1/2}\text{TiO}_3\text{-BaTiO}_3$ ceramics. *J. Eur. Ceram. Soc.* **2002**, *22*, 2115–2121. [[CrossRef](#)]
26. Pan, H.; Zeng, Y.; Shen, Y.; Lin, Y.; Ma, J.; Li, L.; Nan, C. $\text{BiFeO}_3\text{-SrTiO}_3$ thin film as a new lead-free relaxor-ferroelectric capacitor with ultrahigh energy storage performance. *J. Mater. Chem.* **2017**, *5*, 5920–5926. [[CrossRef](#)]
27. Lahmar, A.; Belhadi, J.; El Marssi, M.; Zannen, M.; Khemakhem, H.; Al-Dahoudi, N. Energy storage property of Lead-free $\text{Na}_{0.5}\text{Bi}_{0.5}\text{TiO}_3$ ceramic and thin film. In Proceedings of the 2017 International Conference in Energy and Sustainability in Small Developing Economies (ES2DE), Funchal, Portugal, 10–12 July 2017; pp. 1–4.
28. Cho, S.; Yun, C.; Kim, Y.S.; Wang, H.; Jian, J.; Zhang, W.; Huang, J.; Wang, X.; Wang, H.; MacManus-Driscoll, J.L. Strongly enhanced dielectric and energy storage properties in lead-free perovskite titanate thin films by alloying. *Nano Energy* **2018**, *45*, 398–406. [[CrossRef](#)]
29. Gallegos-Melgar, A.; Espinosa-Arbelaez, D.G.; Flores-Ruiz, F.J.; Lahmar, A.; Dellis, J.L.; Lemée, N.; Espinoza-Beltran, F.J.; Muñoz-Saldaña, J. Ferroelectric properties of manganese doped $(\text{Bi}_{1/2}\text{Na}_{1/2})\text{TiO}_3$ and $(\text{Bi}_{1/2}\text{Na}_{1/2})\text{TiO}_3\text{-BaTiO}_3$ epitaxial thin films. *Appl. Surf. Sci.* **2015**, *359*, 923–930. [[CrossRef](#)]
30. Zhang, Y.L.; Li, W.L.; Cao, W.P.; Zhang, T.D.; Bai, T.R.G.L.; Yu, Y.; Hou, Y.F.; Feng, Y.; Fei, W.D. Enhanced energy-storage performance of $0.94\text{NBT}\text{-}0.06\text{BT}$ thin films induced by a $\text{Pb}_{0.8}\text{La}_{0.1}\text{Ca}_{0.1}\text{Ti}_{0.975}\text{O}_3$ seed layer. *Ceram. Int.* **2016**, *42*, 14788–14792. [[CrossRef](#)]
31. Alonso-Sanjosed, D.; Jiménez, R.; Bretos, I.; Calzada, M.L. Lead-free ferroelectric $(\text{Na}_{1/2}\text{Bi}_{1/2})\text{TiO}_3\text{-BaTiO}_3$ thin films in the morphotropic phase boundary composition: Solution processing and properties. *J. Am. Ceram. Soc.* **2009**, *92*, 2218–2225. [[CrossRef](#)]
32. Badapanda, T.; Sahoo, S.; Nayak, P. Dielectric, Ferroelectric and Piezoelectric study of BNT–BT solid solutions around the MPB region. In Proceedings of the IOP Conference Series: Materials Science and Engineering, Orissa, India, 9–10 December 2017; Volume 178, p. 12032. [[CrossRef](#)]
33. Aissa, M.; Zannen, M.; Alzahrani, H.A.H.; Belhadi, J.; Hadouch, Y.; Mezzane, D.; El Marssi, M.; Majdoub, M.; Lahmar, A. Multifunctionality of rare earth doped $0.925\text{Na}_{0.5}\text{Bi}_{0.5}\text{TiO}_3\text{-}0.075\text{K}_{0.5}\text{Na}_{0.5}\text{NbO}_3$ ferroelectric ceramics. *J. Alloys Compd.* **2022**, *921*, 166188. [[CrossRef](#)]
34. Lahmar, A.; Ehrenberg, H.; Antic-Fidancev, E.; Ganschow, S.; Zriouil, M.; Elouadi, B. Single crystal structure determination and infrared fluorescence of the system $(\text{K}_3\text{Sr}_{1-x}\text{Nd}_x)(\text{Nd}_{1-x}\text{Sr}_{1+x})\text{Nb}_{10}\text{O}_{30}$. *Mater. Res. Bull.* **2012**, *47*, 2566–2572. [[CrossRef](#)]
35. Chahal, R.; Starecki, F.; Doualan, J.-L.; Němec, P.; Trapananti, A.; Prestipino, C.; Tricot, G.; Boussard-Pledel, C.; Michel, K.; Braud, A.; et al. Nd^{3+} : Ga–Ge–Sb–S glasses and fibers for luminescence in mid-IR: Synthesis, structural characterization and rare earth spectroscopy. *Opt. Mater. Express* **2018**, *8*, 1650. [[CrossRef](#)]

Disclaimer/Publisher’s Note: The statements, opinions and data contained in all publications are solely those of the individual author(s) and contributor(s) and not of MDPI and/or the editor(s). MDPI and/or the editor(s) disclaim responsibility for any injury to people or property resulting from any ideas, methods, instructions or products referred to in the content.